

Computing Forward Reachable Sets for Nonlinear Adaptive Multirotor Controllers

Juyeop Han and Han-Lim Choi

Abstract—In multirotor systems, guaranteeing safety while considering unknown disturbances is essential for robust trajectory planning. Computing the forward reachable set (FRS), the set of all possible states with bounded disturbances, can be a viable solution to find robust and collision-free trajectories. However, in many cases, the FRS is not calculated in real time and is too conservative to be used in actual applications. In this paper, we mitigate these problems by applying a nonlinear disturbance observer (NDOB) and an adaptive controller to the multirotor system. We formulate the FRS of the closed-loop system combined with the adaptive controller in augmented state space by exploiting the Hamilton-Jacobi reachability analysis and then present the ellipsoidal approximation in a closed-form expression to compute the small FRS in real time. Moreover, tighter disturbance bounds in the prediction horizon are inferred from the NDOB so that a much smaller FRS can be generated. Numerical examples validate the computational efficiency and the smaller scale of the proposed FRS compared to the baseline.

I. INTRODUCTION

Recently, multicopters have attracted attention due to their agile maneuvers, simple dynamics, and potential for complex tasks, such as surveillance [1] and aerial manipulation [2]. Mostly, safety in the multicopter is referred to as avoiding various obstacles and is indispensable to prevent catastrophic accidents. Sampling-based motion planning, such as the rapidly exploring random tree (RRT) algorithm [3], samples free points in the configuration space and searches for a collision-free path. [4], [5] exploit convex optimization and motion primitives to generate a feasible and collision-free trajectory for a multicopter. However, these approaches do not fully guarantee safety as a result of unexpected factors, such as air drags, wind gusts, and model uncertainty, which cause disturbances in the actual system dynamics.

Therefore, safety should be ensured by considering disturbances when planning the trajectory of a multicopter. The forward reachable set (FRS) is one of the most popular concepts for analyzing the safety of the system dynamics. A FRS is a set of all states produced by all possible bounded disturbances given an initial state set.

The Hamilton-Jacobi (HJ) reachability analysis is a method for computing reachable sets based on an optimal

This research was supported by Unmanned Vehicles Core Technology Research and Development Program through the National Research Foundation of Korea(NRF), Unmanned Vehicle Advanced Research Center(UVARC) funded by the Ministry of Science and ICT, the Republic of Korea (2020M3C1C1A01082375)

Juyeop Han and Han-Lim Choi are with the KAIST Institutes for Robotics and the Department of Aerospace Engineering, Korea Advanced Institute of Science and Technology (KAIST), Daejeon, 34141, South Korea. jyhan@ics.kaist.ac.kr, hanlimc@kaist.ac.kr

control theory [6]. The HJ partial differential equation (PDE) for the sub-level set is derived by the principle of dynamic programming. However, the HJ reachability analysis is associated with the "curse of dimensionality;" that is, solving the HJ PDE requires computation exponential to the number of states of the system [7]. To resolve and mitigate this issue, the decomposition of the system dynamics [8] and a deep-learning-based approach [9] can be applied. Many studies without using the HJ reachability analysis provide a method by which to determine the outer or inner approximation of an exact FRS of a linear system to well-known geometric shapes, such as a zonotope [10] or an ellipsoid [11], [12], as it is intractable to attempt to find the exact FRSs of many high-dimensional nonlinear systems.

Trajectory planning guaranteeing safety against disturbances can be performed by combining existing planning approaches and the forward reachable set including the FRS. [13] computes the FRSs of motion primitives, referred to as a funnel, using sums of squares (SOS) programming and utilizes these funnels for trajectory planning. [14] designs a multirotor controller compensating for aerodynamic effects and computes tight FRSs by SOS programming as well. [15], [16] convert a robust trajectory planning problem into a pursuit-evasion game. The maximum tracking error is computed via a HJ reachability analysis and is utilized to avoid obstacles. All of these studies require an offline phase for the FRS computation. On the other hand, [17], [18] compute the FRSs of the nominal trajectories of the multirotor in real time. These studies approximate the FRS to an ellipsoid in an analytical expression by exploiting a generalized Hopf formula [19]. Although [17], [18] compute the high dimensional approximation of the FRS in real time unlike [10], [11], [12], the approximated FRS is too conservative to be applied to agile trajectory planning.

Our research aims to compute small FRSs in a receding horizon using a nonlinear disturbance observer (NDOB) and a nonlinear adaptive controller for a multirotor in real time. To achieve this objective, we extend earlier work [17], [18] by applying the adaptive controller as a feedback controller with the assumption that the disturbance is differentiable and that its time derivative is bounded. The NDOB and the adaptive controller for the multirotor are presented and the stability is proven to justify their use in the first step of this paper. Tight future disturbance bounds are predicted by the NDOB for the computation of the smaller FRSs. Moreover, we augment the estimated disturbance and true disturbance to the closed-loop dynamics of the multirotor. The FRSs of the augmented dynamics are formulated by a

HJ reachability analysis and are approximated to ellipsoids. Finally, the ellipsoidal FRSs are projected onto the original state space in an analytical expression.

The main contributions of the paper are as follows:

- a mathematical formulation of the FRSs and their ellipsoidal over-approximation is proposed in the augmented state space and the FRSs of the multirotor system combined with the adaptive controller are computed.
- the approximated FRSs are computed in real time and are much smaller than a baseline [18] when tightening future possible disturbances and adding the NDOB and the adaptive controller to the multirotor system.

A. Notation

In this paper, $(\cdot)_i$ denotes the i -th element of a vector. $\mathbf{0}_{n \times m} \in \mathbb{R}^{n \times m}$ and $I_n \in \mathbb{R}^{n \times n}$ are correspondingly a $n \times m$ zero matrix and a $n \times n$ identity matrix. $\|\cdot\|$ and $\|\cdot\|_\infty$ likewise represent a second norm and a ∞ -norm. $\text{Proj}_{\mathbb{A}}(\cdot)$ and $\text{Prop}_{\mathbb{A}}(\cdot)$ are the set projection and propagation operation to the space \mathbb{A} . $\mathbb{E}(s, K) = \{x \in \mathbb{R}^n \mid (x - s)^T K (x - s) \leq 1\}$ is an ellipsoid for a vector $s \in \mathbb{R}^n$ and a positive definite matrix $K \in \mathbb{R}^{n \times n}$. Finally, \oplus stands for the Minkowski sum between two sets, and \bigoplus represents a series of the Minkowski sums of multiple sets.

II. PROBLEM FORMULATION

We denote the simplified state and control input of the multirotor dynamics as $x = [p^T \ v^T \ \Phi^T]^T \in \mathbb{X} \subset \mathbb{R}^9$ and $u = [F \ \omega^T]^T \in \mathbb{U} \subset \mathbb{R}^4$. The position, the velocity and the Euler angle are represented as $p \in \mathbb{R}^3$, $v \in \mathbb{R}^3$ and $\Phi \in \mathbb{R}^3$, respectively. $F \in \mathbb{R}$ and $\omega \in \mathbb{R}^3$ are likewise the normalized thrust and the angular velocity of the multirotor. We consider the simplified multirotor dynamics with disturbance $d \in \mathbb{R}^3$ as a control-affine form:

$$\dot{x} = f(x) + g_1(x)u + g_2d \quad (1)$$

with

$$\begin{aligned} f(x) &= [v^T \ (-ge_3)^T \ \mathbf{0}_{1 \times 3}]^T \\ g_1(x) &= \begin{bmatrix} \mathbf{0}_{1 \times 3} & (R(\Phi)e_3)^T & \mathbf{0}_{1 \times 3} \\ \mathbf{0}_{3 \times 3} & \mathbf{0}_{3 \times 3} & C(\Phi)^T \end{bmatrix} \\ g_2 &= [\mathbf{0}_{3 \times 3} \ I_3 \ \mathbf{0}_{3 \times 3}]^T \end{aligned}$$

denoting the magnitude of gravity acceleration $g \in \mathbb{R}$, and $e_3 = [0 \ 0 \ 1]^T \in \mathbb{R}^3$. $R(\Phi) \in \mathbb{R}^{3 \times 3}$ is the rotation matrix from the body frame to the inertial frame. $C(\Phi)$ is the mapping matrix from the angular velocity to the Euler angle rate. In this paper, we assume the following characteristics of disturbances:

Assumption 1. *The disturbance vector and its time derivative are bounded by positive real constants in each channel. That is, the disturbance at time t is an element of*

$$\mathcal{D}(t) = \{d(t) \mid \forall \tau \in [t_0, t], \exists w(\tau) \in \mathcal{W}, \dot{d}(\tau) = w(\tau), |d_i(\tau)| \leq L_i, d(t_0) \in \mathcal{D}(t_0)\} \quad (2)$$

with $\mathcal{W} = \{w \mid |w_i| \leq \beta_i\} \subset \mathbb{R}^3$, and constant vectors, $L \in \mathbb{R}^3$ and $\beta \in \mathbb{R}^3$.

We also consider a nonlinear disturbance observer (NDOB) as the dynamics of the estimated disturbance $\hat{d} \in \mathbb{R}^3$:

$$\dot{\hat{d}} = \zeta(\hat{d}, d) \quad (3)$$

The exact system formulation of the NDOB will be described in Section III-A. Furthermore, the dynamics of the estimated disturbance will be shown to be linear.

Subsequently, we build an adaptive controller to compensate for the estimated disturbance and to track a differential flat output, $\sigma(t) = [p_r(t)^T \ \psi_r(t)]^T \in \mathbb{R}^4$, where $p_r(t) \in \mathbb{R}^3$ and $\psi_r(t) \in \mathbb{R}$ are correspondingly the reference position and yaw angle [4]. The closed-loop dynamics combined with the adaptive controller can be expressed as

$$\begin{aligned} u(t) &= \kappa(x(t), \hat{d}(t); \sigma(t)) \\ \dot{x}(t) &= h(x(t), \hat{d}(t); \sigma(t)) + g_2d(t) \end{aligned} \quad (4)$$

where $\kappa(x(t), \hat{d}(t); \sigma(t))$ is the adaptive controller, and $h(x(t), \hat{d}(t); \sigma(t)) = f(x(t)) + g_1(x(t))\kappa(x(t), \hat{d}(t); \sigma(t))$. The exact formulation of κ will be described in Section III-A as well.

Let us define the FRS of the closed-loop dynamics at time t , $\mathcal{X}(t) \subset \mathbb{X}$, as follows:

$$\begin{aligned} \mathcal{X}(t) &= \{x(t) \mid \forall \tau \in [t_0, t], \exists d(\tau) \in \mathcal{D}(\tau), \\ &\quad \dot{x}(\tau) = h(x(\tau), \hat{d}(\tau); \sigma(\tau)) + g_2d(\tau), \\ &\quad \dot{\hat{d}}(\tau) = \zeta(\hat{d}(\tau), d(\tau)), \\ &\quad x(t_0) \in \mathcal{X}(t_0), \hat{d}(t_0) \in \hat{\mathcal{D}}_0\} \end{aligned} \quad (5)$$

where $\hat{\mathcal{D}}_0$ is the initial set of the estimated disturbance.

The objective of the research is to compute the approximation of the FRS, $\mathcal{X}(\tau)$, in receding horizon $\tau \in [t_0, t_f]$ in real time.

III. NONLINEAR DISTURBANCE OBSERVER AND ADAPTIVE CONTROLLER

A. Nonlinear Disturbance Observer and Adaptive Controller Design

The structure of the NDOB for the multirotor dynamics (1) introduces an internal state vector $z \in \mathbb{R}^3$ to estimate the true disturbance d [20]:

$$\begin{aligned} \dot{d} &= z + p(x) \\ \dot{z} &= -L_d(x)g_2z - L_d(x)[f(x) + g_1(x)u + g_2p(x)] \end{aligned} \quad (6)$$

with $p(x) = \alpha_d v \in \mathbb{R}^3$ and $L_d(x) = \partial p / \partial x = \alpha_d g_2^T \in \mathbb{R}^{3 \times 9}$. $\alpha_d \in \mathbb{R}$ is a positive real constant. Let $e_d = d - \hat{d}$ be the disturbance error. The estimated disturbance dynamics $\dot{\hat{d}} = \zeta(\hat{d}, d)$ is derived as $\dot{\hat{d}} = \alpha_d e_d$ by differentiating (6).

At this point, we design the adaptive controller κ to compensate for the estimated disturbance \hat{d} in a manner similar to that in [14]. Let $e_p = p - p_r$ and $e_v = v - \dot{p}_r$ be the position error and the velocity error, respectively. The thrust of the adaptive controller is expressed as

$$\begin{aligned} f_d &= -k_p e_p - k_v e_v + ge_3 + \ddot{p}_r - \hat{d} \\ \mathbf{z}_{\mathbf{b}, \mathbf{d}} &= \frac{f_d}{\|f_d\|}, \quad f = f_d^T \mathbf{z}_{\mathbf{b}} = \|f_d\| \mathbf{z}_{\mathbf{b}, \mathbf{d}}^T \mathbf{z}_{\mathbf{b}} \end{aligned} \quad (7)$$

where $k_p \in \mathbb{R}$ and $k_v \in \mathbb{R}$ are the positive feedback gains and \mathbf{z}_b is the thrust direction of the multirotor. The desired roll $\phi_r(t)$ and pitch $\theta_r(t)$ can be computed from the thrust (7) and the flat output $\sigma(t)$ [4]. The angular velocity ω is controlled to follow the reference Euler angle $\Phi_r(t) \in \mathbb{R}^3$ according to the attitude controller having exponential stability, such as the geometric controller [21], [22].

Suppose that ϕ_b is the angle between the desired thrust direction $\mathbf{z}_{b,d}$ and the true thrust direction \mathbf{z}_b . Because the controller makes the attitude error exponentially stable, the angle $\phi_b \in \mathbb{R}$ is bounded so that there exists s_m such that $|\sin \phi_b| \leq s_m$ if the initial attitude is close to the initial reference attitude.

B. Uniformly Ultimate Boundedness

The dynamics of the position error and the velocity error of the closed-loop and the disturbance error dynamics of the NDOB are derived as

$$\begin{aligned}\dot{e}_p &= e_v \\ \dot{e}_v &= -k_p e_p - k_v e_v + e_d + (\|f_d\| \sin \phi_b) \mathbf{w} \\ \dot{e}_d &= w - \alpha_d e_d\end{aligned}\quad (8)$$

where $\mathbf{w} \in \mathbb{R}^3$ is the unit vector of $(\mathbf{z}_b \cdot \mathbf{z}_{b,d}) \mathbf{z}_b - \mathbf{z}_{b,d}$.

We show that the error of (8) is uniformly ultimately bounded (UUB) to verify the convergence of the presented adaptive controller.

Lemma 1. *The disturbance error dynamics e_d is UUB.*

proof: See Appendix A. \square

The rate and radius of convergence in *Lemma 1* will be used for estimating tight disturbance bound prediction in Section IV-B.

Proposition 1. *The dynamics of the position error e_p and the velocity error e_v are UUB if $k_v > 1$, $\alpha_d > \frac{1}{4}(\frac{1}{k_p} + \frac{1}{k_v-1})$ and $s_m < -\lambda_{\min}(Q_1)/\lambda_{\min}(Q_2)$, where $\lambda_{\min}(Q_1)$ and $\lambda_{\min}(Q_2)$ are the corresponding minimum eigenvalues of Q_1 and Q_2 , and*

$$Q_1 = \begin{bmatrix} k_p & 0 & -\frac{1}{2} \\ 0 & k_v - 1 & -\frac{1}{2} \\ -\frac{1}{2} & -\frac{1}{2} & \alpha_d \end{bmatrix},$$

$$Q_2 = \begin{bmatrix} -k_p & -\frac{1}{2}(k_p + k_v) & -\frac{1}{2} \\ -\frac{1}{2}(k_p + k_v) & -k_v & -\frac{1}{2} \\ -\frac{1}{2} & -\frac{1}{2} & 0 \end{bmatrix}$$

proof: See Appendix B. \square

C. Disturbance Bound Prediction on the Prediction Horizon

Suppose that the initially estimated disturbance is set to $\hat{d}(0) = \mathbf{0}_{3 \times 1}$ and that the disturbance d is observed during time interval $[0, t_0]$ by the NDOB (6). Let future possible disturbance predictions start from time t_0 for the FRS computation. We derive the ∞ -norm bound of the disturbance error at time t_0 , $\|e_d(t_0)\|_\infty \leq r(t_0)$, from the proof of the *Lemma 1* with $r(t) = \max(\|L\| \exp[-(1 - \theta_1)\alpha_d t], \|\beta\|/(\theta_1\alpha_d))$.

Given that the disturbances and their time derivatives are bounded to the constant vector radius L and β according to the *Assumption 1*, for the future possible disturbance set, the following inclusive relationship for all $\tau \in [t_0, t]$ applies:

$$\begin{aligned}\mathcal{D}(\tau) &\subset \mathcal{D}_{\mathcal{F}}(\tau) \cap \mathcal{D}_{\mathcal{B}} \\ \text{s.t. } \mathcal{D}_{\mathcal{B}} &= \{d \mid |d_i| \leq L_i\} \\ \mathcal{D}_{\mathcal{F}}(\tau) &= \{d(\tau) \mid |d(\tau) - \hat{d}_i(t_0)| \leq r(t_0) + \beta_i(\tau - t_0)\}\end{aligned}\quad (9)$$

We set the upper and lower bounds of i -th channel of $\mathcal{D}_{\mathcal{F}}(\tau) \cap \mathcal{D}_{\mathcal{B}}$ to $d_{L,i}(\tau)$ and $d_{U,i}(\tau)$. Let the center and the edge of the future disturbance be $d_m(\tau) \in \mathbb{R}^3$ and $d_M(\tau) \in \mathbb{R}^3$, where the i -th elements of these vectors are $d_{m,i}(\tau) = (d_{L,i}(\tau) + d_{U,i}(\tau))/2$ and $d_{M,i}(\tau) = (d_{U,i}(\tau) - d_{L,i}(\tau))/2$, respectively. As a result, the future possible disturbances at time t are expressd as

$$\mathcal{D}_P(t) = \{d(t) \mid \forall \tau \in [t_0, t], |d_i(\tau) - d_{m,i}(\tau)| < d_{M,i}(\tau)\} \quad (10)$$

and, the relationship, $\text{Prop}_{\mathbb{Y}}(\mathcal{D}(t)) \subset \text{Prop}_{\mathbb{Y}}(\mathcal{D}_P(t))$, is satisfied.

IV. ADAPTIVE FORWARD REACHABLE SET COMPUTATION

A. System Linearization with State Augmentation and Forward Reachable Sets

The original Hamilton-Jacobi (HJ) reachability analysis is not designed to compute reachable sets considering the NDOB (6) and the differentiability of the disturbance d . Therefore, the estimated disturbance \hat{d} and the real disturbance d are added to the state x to compute the FRS (5) considering these characteristics through a HJ reachability analysis.

Let $y = [x^T \ \hat{d}^T \ d^T]^T \in \mathbb{Y} \subset \mathbb{R}^{15}$ be the augmented state of the multirotor. From (2), (3) and (4), the dynamics of the augmented state y is derived as

$$\begin{aligned}\dot{y}(t) &= \begin{bmatrix} h(x(t), \hat{d}(t); \sigma(t)) + g_2 d(t) \\ -\alpha_d \hat{d}(t) + \alpha_d d(t) \\ \mathbf{0}_{3 \times 1} \end{bmatrix} + F w(t) \\ &= \xi(y(t); \sigma(t)) + F w(t)\end{aligned}\quad (11)$$

with $F = [\mathbf{0}_{3 \times 12} \ I_3]^T \in \mathbb{R}^{15 \times 3}$. The error of the augmented dynamics (11) can be linearized to apply the generalized Hopf formula [19] in Section IV-B to compute the FRS of the augmented dynamics:

$$\dot{e}_y(t) = A(t) e_y(t) + F w(t) + \mu(y(t), w(t); \sigma(t)) \quad (12)$$

with $e_y(t) = y(t) - y_r(t)$, $A(t) = \partial \xi / \partial y|_{(y_r(t); \sigma(t))}$, the linearization error $\mu(y(t), w(t); \sigma(t)) = [\Delta_p^T \ \Delta_v^T \ \Delta_\Phi^T \ \mathbf{0}_{6 \times 1}^T]^T$, $\Delta_p \in \mathbb{R}^3$, $\Delta_v \in \mathbb{R}^3$, and $\Delta_\Phi \in \mathbb{R}^3$. $y_r(t) \in \mathbb{Y}$ is a zero-disturbance reference state with initial condition $y_r(t_0) = y(t_0)$ such that $\forall \tau \in (t_0, t]$, $d_r(\tau) = \mathbf{0}_{3 \times 1}$ and $\dot{y}_r(\tau) = \xi(y_r(\tau); \sigma(\tau))$.

Assumption 2. *The linearization error $\mu(y(t), w(t); \sigma(t))$ is neglected or bounded to $M_y = [M_p^T \ M_v^T \ M_\Phi^T \ \mathbf{0}_{6 \times 1}^T]^T \in$*

\mathbb{R}^{15} with maximum errors of the position, velocity, and the Euler angle, $M_p \in \mathbb{R}^3$, $M_v \in \mathbb{R}^3$, $M_\Phi \in \mathbb{R}^3$, respectively.

According to *Assumption 2*, the error dynamics (12) becomes

$$\dot{e}_y(t) = A(t)e_y(t) + \bar{F}\bar{w}(t) \quad (13)$$

with $\bar{w} = w$ and $\bar{F} = F$ when the linearized error is neglected, or $\bar{w} = [\Delta_p^T \Delta_v^T \Delta_\Phi^T w^T]^T \in \mathbb{R}^{12}$ and $\bar{F} = [F' \ F] \in \mathbb{R}^{15 \times 12}$ with $F' = [I_9 \ \mathbf{0}_{9 \times 6}]^T \in \mathbb{R}^{15 \times 9}$ when the linearized error is considered and bounded. To avoid confusion, let $n_{\bar{w}}$ be a dimension of \bar{w} ; i.e., $n_{\bar{w}} = 3$ or $n_{\bar{w}} = 12$ for each case. The vector \bar{w} is bounded to the vector $\bar{\beta} \in \mathbb{R}^{n_{\bar{w}}}$ with $\bar{\beta} = \beta \in \mathbb{R}^3$ when the linearization error is neglected, or $\bar{\beta} = [M_p^T \ M_v^T \ M_\Phi^T \ \beta^T]^T \in \mathbb{R}^{12}$ when the linearization error is considered and bounded. $\bar{\mathcal{W}}$ is defined as a set of all possible vectors \bar{w} . As a result, the vector \bar{w} can be shown as the bounded disturbance of (13).

The FRS of the linearized error dynamics (12) without considering the possible disturbance set $\mathcal{D}(t)$ is defined as shown below.

$$\begin{aligned} \mathcal{E}_y(t) &= \{e_y(t) \mid \forall \tau \in [t_0, t], \exists w(\tau) \in \mathcal{W}(\tau), \\ \dot{e}_y(\tau) &= A(\tau)e_y(\tau) + \bar{F}\bar{w}(\tau), e_y(t_0) \in \mathcal{E}_y(t_0)\} \end{aligned} \quad (14)$$

Because $\mathcal{E}_y(t) \cap \text{Prop}_{\mathbb{Y}}(\mathcal{D}(t))$ represents the FRS of the error dynamics considering the disturbance set $\mathcal{D}(t)$, the FRS of the augmented dynamics (11) is $y_r(t) + \mathcal{E}_y(t) \cap \text{Prop}_{\mathbb{Y}}(\mathcal{D}(t))$, which is a translation of the FRS of the augmented error dynamics with the augmented reference state $y_r(t)$.

According to the definition of \mathcal{X} (5) and \mathcal{E}_y (14), the following relationship is satisfied if the projection of $\mathcal{E}_y(t_0) \cap \text{Prop}_{\mathbb{Y}}(\mathcal{D}(t_0))$ to the original state space \mathbb{X} and the projection to the estimated disturbance space are correspondingly identical to $\mathcal{X}(t_0)$ and $\hat{\mathcal{D}}_0$:

$$\begin{aligned} \mathcal{X}(t) &= x_r(t) + \text{Proj}_{\mathbb{X}}(\mathcal{E}_y(t) \cap \text{Prop}_{\mathbb{Y}}(\mathcal{D}(t))) \\ &\subset x_r(t) + \text{Proj}_{\mathbb{X}}(\mathcal{E}_y(t) \cap \text{Prop}_{\mathbb{Y}}(\mathcal{D}_P(t))) \end{aligned} \quad (15)$$

with $x_r(t) = \text{Proj}_{\mathbb{X}}(y_r(t))$.

B. Coordinate Transformation and Hamilton-Jacobi Reachability Analysis

We aim to approximate $\mathcal{E}_y(t) \cap \text{Prop}_{\mathbb{Y}}(\mathcal{D}_P(t))$ to an ellipsoid in a way similar to that in [17], [18]. Suppose that $\mathcal{E}_y(t)$ is the sub-zero level set of the value function $V(e_y, t) \in \mathbb{R}$:

$$\mathcal{E}_y(t) = \{e_y \mid V(e_y, t) \leq 0\} \text{ s.t. } \mathcal{E}_y(t_0) = \{s \mid l_0(s) \leq 0\} \quad (16)$$

where $l_0(s) \in \mathbb{R}$ is the initial convex value function. Let $l_0(s) = (s - q_0)^T Q_0^{-1}(s - q_0) - 1$ so that $\mathcal{E}_y(t_0) = \mathbb{E}(q_0, Q_0^{-1})$ for vector $q_0 \in \mathbb{R}^{15}$ and positive definite matrix $Q_0 \in \mathbb{R}^{15 \times 15}$.

By multiplying the state transition matrix $\Psi(t)$ by the error dynamics (13), the system is transformed to a new dynamics for the variable $\eta(t) = \Psi^{-1}(t)e_y(t)$:

$$\dot{\eta}(t) = \Psi^{-1}(t)\bar{F}\bar{w}(t) = \bar{F}_\eta(t)\bar{w}(t). \quad (17)$$

The HJ reachability analysis [7] provides the following HJ partial differential equation to find the value function $V_\eta(\eta, t)$:

$$\begin{aligned} \frac{\partial V_\eta}{\partial t} + H\left(\frac{\partial V_\eta}{\partial \eta}, t\right) &= 0 \\ V_\eta(\eta, t_0) &= l_{0,\eta}(\eta) \\ H_\eta(p, t) &= \max_{\bar{w}(t) \in \bar{\mathcal{W}}} p^T (\bar{F}_\eta(t)\bar{w}(t)) \end{aligned} \quad (18)$$

where $(\cdot)_\eta$ denotes the corresponding formulation of (\cdot) in η -space. The following explicit solution of (18) is found by the generalized Hopf formula:

$$\begin{aligned} \mathcal{E}_\eta(t) &= \mathcal{E}_Y(t_0) \oplus \mathcal{G}_\eta(t) \\ \text{s.t. } \mathcal{G}_\eta(t) &= \bigoplus_{i=1}^{n_{\bar{w}}} \mathcal{G}_{\eta,i}(t) \\ \mathcal{G}_{\eta,i}(t) &= \left\{ \bar{\beta}_i \int_{t_0}^t \bar{F}_{\eta,i}(\tau) \text{sign}(Q_0^{-\frac{1}{2}} \bar{F}_{\eta,i}(\tau)^T \nu) d\tau \mid \|\nu\|^2 \leq 1 \right\} \end{aligned} \quad (19)$$

where $\bar{F}_{\eta,i}(t)$ is the i -th column of $\bar{F}_\eta(t)$. For more detailed information, we refer the reader to [17], [18].

C. Ellipsoidal Approximation

Set $\mathcal{G}_\eta(t)$ is approximated to the ellipsoid $\mathbb{E}(\mathbf{0}_{15 \times 1}, B_\eta^{-1}(t))$ [17], [18], as shown below.

$$\begin{aligned} \mathcal{G}_\eta(t) &\subset \mathbb{E}(\mathbf{0}_{15 \times 1}, B_\eta^{-1}(t)) \\ \text{s.t. } B_\eta(t) &= \sum_{i=1}^{n_{\bar{w}}} \frac{B_{\eta,i}(t)}{a_i} \end{aligned} \quad (20)$$

$$B_{\eta,i}(t) = (t - t_0) \int_{t_0}^t (\bar{\beta}_i^2 \bar{F}_{\eta,i}(\tau) \bar{F}_{\eta,i}(\tau)^T + \epsilon I_{15}) d\tau$$

where $a_i = \sqrt{\text{tr}(B_{\eta,i}(t))} / (\sum_{i=1}^{n_{\bar{w}}} \sqrt{\text{tr}(B_{\eta,i}(t))})$ is a coefficient that enables $B_\eta(t)$ to be a minimal-trace containing the sum of ellipsoids [23] and ϵ is any positive constant.

According to (19) and (20), a conservative ellipsoidal approximation of $\mathcal{E}_\eta(t)$ satisfies $\mathcal{E}_\eta(t) \subset \mathbb{E}(\mathbf{0}_{15 \times 1}, Q_\eta^{-1}(t))$ with $Q_\eta(t) = Q_0/a_1 + B_\eta(t)/a_2$, where the coefficients, a_1 and a_2 are designed for ellipsoidal fusion with the minimal trace as (20). Next, $\mathbb{E}(\mathbf{0}_{15 \times 1}, Q_\eta^{-1}(t))$ is converted to the approximation of $\mathcal{E}_y(t)$ in e_y -space; i.e., $\mathcal{E}_y(t) \subset \mathbb{E}(\mathbf{0}_{15 \times 1}, Q_y^{-1}(t))$ where $Q_y(t) = \Psi(t)Q_\eta(t)\Psi(t)^T$.

We approximate $\mathcal{D}_P(t)$ to a conservative ellipsoid, $\mathbb{E}(d_m(t), \Lambda(t))$ with $\Lambda = \text{diag}([\lambda_1, \lambda_2, \lambda_3])$. For $\Lambda^{-1}(t)$ to have a minimal trace, a convex problem (21) is shown below and solved by applying the KKT condition [24].

$$\min_{\lambda_i} \sum_{i=1}^3 \frac{1}{\lambda_i} \text{ s.t. } \sum_{i=1}^3 \lambda_i d_{M,i}^2 \leq 1 \quad (21)$$

The optimal matrix having a minimal inverse trace is $\Lambda^* = \text{diag}([\lambda_1^*, \lambda_2^*, \lambda_3^*])$ with $\lambda_i^* = (\sum_{j=1}^3 d_{M,j})^{-1} d_{M,i}^{-1}$.

As a result, we can express $\mathcal{E}_y(t) \cap \text{Prop}_{\mathbb{Y}}(\mathcal{D}_P(t))$ as a conservative approximation of the intersections of ellipsoids:

$$\begin{aligned} \mathcal{E}_y(t) \cap \text{Prop}_{\mathbb{Y}}(\mathcal{D}_P(t)) &\subset \\ \mathbb{E}(0, Q_y^{-1}(t)) \cap \text{Prop}_{\mathbb{Y}}(\mathbb{E}(d_m(t), \Lambda^*(t))) & \end{aligned} \quad (22)$$

Note that the propagation of the ellipsoid to higher dimension space can be represented in the form of an ellipsoid by adding zeros to the elements of its center and matrix corresponding to the propagated dimensions. Let $d_m^Y(t) \in \mathbb{R}^{15}$ and $\Lambda^Y(t) \in \mathbb{R}^{15 \times 15}$ be the corresponding center and matrix of $\text{Prop}_Y(\mathbb{E}(d_m(t), \Lambda^*(t)))$.

We again approximate (22) to a single ellipsoid [23]:

$$\begin{aligned} S(t) &= \mathbb{E}(c(t), M(t)) \\ \text{s.t. } c(t) &= (1-b)N^{-1}\Lambda^Y(t)d_m^Y(t), \quad M(t) = \frac{N(t)}{1-\delta}, \quad (23) \\ N(t) &= bQ_y^{-1}(t) + (1-b)\Lambda^Y(t), \\ \delta &= (1-b)(d_m^Y(t))^T\Lambda^Y(t)d_m^Y(t) - c^T N c \end{aligned}$$

with $0 \leq b \leq 1$. The ellipsoid $S(t)$ is utilized for the initial ellipsoid $\mathbb{E}(q_0, Q_0^{-1})$ to calculate the propagated $S(t + \Delta t)$ after time step Δt .

Finally, the approximation of the FRS (15) is derived from the projection of (23) to the original state space \mathbb{X} as $x_r(t) + \text{Proj}_{\mathbb{X}}(S(t))$. $\text{Proj}_{\mathbb{X}}(S(t))$ is an ellipsoid [25] and can be represented as

$$\mathbb{E}(\text{Proj}_{\mathbb{X}}(c(t)), M_{11}(t) - M_{12}(t)M_{22}^{-1}(t)M_{21}(t)), \quad (24)$$

where $M_{11}(t) \in \mathbb{R}^{9 \times 9}$, $M_{12}(t) \in \mathbb{R}^{9 \times 6}$, $M_{21}(t) \in \mathbb{R}^{6 \times 9}$ and $M_{22}(t) \in \mathbb{R}^{6 \times 6}$ are block components of $M(t)$ divided by the original state x and the disturbance state $[\hat{d}^T \quad d^T]^T$.

V. NUMERICAL EXAMPLES

We implement two numerical scenarios to verify our method for FRS computations on a desktop computer. All scenarios are designed to verify the small trace and volume of the FRS computed by our method compared to that of the FRS computed by the baseline [18] with the controller which is identical to the controller introduced in Section. III except that the estimated disturbance \hat{d} is always set to zero.

A. Setup and Scenarios

The computer has an Intel Core i7-8700 CPU with a 3.2GHz base clock and 32GB of RAM. The computation method is programmed in MATLAB R2020b on Linux 18.04. The reference trajectory in all examples is a circular trajectory rotated with a 30° roll and a 30° yaw. The center of the trajectory is $[0 \ 0 \ 0]^T$. The radius of the trajectory is 10m and 0.6 rad/s, in the two cases. We compute the FRSs with a 2.7s prediction horizon. The parameters used in the numerical examples are shown in Table I. We set the disturbance bound L to describe the wind blowing from the lateral direction. K denotes a vector composed of feedback gains including the position and velocity feedback gain, k_p and k_v in Section III. $q_0(t_0)$ and $Q_0(t_0)$ denote the center of an ellipsoid and the inverse ellipsoidal matrix representing the initial set at the initial time, t_0 , of the prediction horizon, respectively.

Scenario 1 shows that the FRSs were computed in the first prediction horizon by the proposed method with or without considering the linearization error and the baseline [18]. Here, 500 trajectories starting from the same points were

TABLE I: Parameters for Numerical Examples

Parameter	Value
α_d	$2.0/\text{s}^2$
θ_1	0.8
Δt	0.02s
b	0.99
K	$[18.0 \ 6.0 \ 7.0 \ 21.0]^T$
L	$[3.0\text{m/s}^2 \ 3.0\text{m/s}^2 \ 1.0\text{m/s}^2]$
β	$[2.0\text{m/s}^3 \ 2.0\text{m/s}^3 \ 2.0\text{m/s}^3]$
M_p	$[0.001\text{m/s} \ 0.001\text{m/s} \ 0.001\text{m/s}]^T$
M_v	$[0.01\text{m/s}^2 \ 0.01\text{m/s}^2 \ 0.01\text{m/s}^2]^T$
M_Φ	$[0.01\text{rad/s} \ 0.01\text{rad/s} \ 0.01\text{rad/s}]^T$
$q_0(t_0)$	$[0\text{m} \ 0\text{m} \ 0\text{m} \ 0\text{m/s} \ 0\text{m/s} \ 0\text{rad} \ 0\text{rad} \ 0\text{rad} \ 0\text{m/s}^2 \ 0\text{m/s}^2 \ 0\text{m/s}^2 \ d_{m,1}(t_0) \ d_{m,2}(t_0) \ d_{m,3}(t_0)]^T$
$Q_0(t_0)$	$\text{diag}([0.05\text{m}, 0.05\text{m}, 0.05\text{m}, 0.05\text{m/s}, 0.05\text{m/s}, 0.05\text{m/s}, 0.05\text{rad}, 0.05\text{rad}, 0.05\text{rad}, 0.05\text{m/s}^2, 0.05\text{m/s}^2, 0.05\text{m/s}^2, 3d_{M,1}(t_0), 3d_{M,2}(t_0), 3d_{M,3}(t_0)])^2$

generated with random disturbances satisfying *Assumption 1*. In Scenario 2, multirotors with the two different controllers used to the baseline and the proposed method followed the reference trajectory within 15.2s. The FRSs computed by the proposed method considering the linearization error and those by [18] were computed every 2.5s. The starting positions were identical to the reference starting position in all scenarios.

B. Results

Fig. 1 illustrates the possible error bounds obtained from the FRSs and the sampled trajectory errors in the position, velocity, and Euler angle in the first scenario. Fig. 2 describes the trace and the determinant of the inverse matrices of the ellipsoidal FRSs in Scenario 1 as Fig. 1. Fig. 3 visualizes the FRSs in the position space and trajectories following the reference trajectories with the two controllers in Scenario 2.

Fig. 1 shows that all sampled trajectories belong to the possible error bound generated by the baseline [18] and the proposed method with or without considering linearization errors. All figures verify that the FRS calculated by our method is much smaller than the baseline FRS [17] on a log scale. Moreover, in Scenario 2, the average computation times for propagation of FRSs of the baseline [18] and of the proposed method when neglecting or considering linearization errors are 13.7ms and 32.7ms, respectively. Although the computation time of the proposed method is slightly slower than that of the baseline [18], our method is fast enough for real-time trajectory planning considering disturbances.

In conclusion, the results verify that the FRS computed by the proposed method is much smaller than the baseline FRS and is implemented in real time.

VI. CONCLUSION

In this paper, we proposed a real-time computation method for a small forward reachable set (FRS) to guarantee the safety of multirotor dynamics with disturbances. We introduce an nonlinear disturbance observer (NDOB) and an adaptive controller into the system dynamics and approximate the FRS to an ellipsoid in an analytical expression.

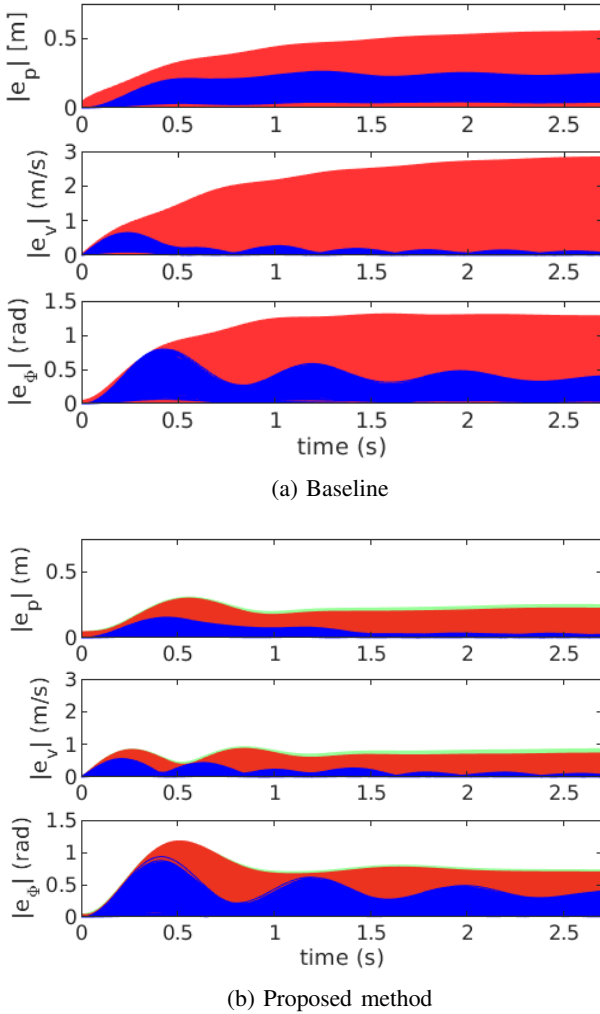


Fig. 1: The maximum error bounds and actual errors obtained from baseline [18] (a) and our method (b) are presented. The possible error bounds neglecting linearization errors (red shaded areas). The additional possible error bounds considering linearization errors (green shaded area). The magnitude of actual state errors (blue area).

Numerical examples verify that the proposed method rapidly computes the smaller FRS of the multirotor system than the baseline [18] does. Also, our approach can be extended to other mobile system dynamics, such as ground vehicles. One limitation is that the FRS is only available when the linearization error of the system is negligible or when the error is bounded and known. Considering the smaller FRS computed by the proposed method than the baseline, the proposed method is highly applicable to plan agile and robust trajectories in real time.

REFERENCES

[1] K. Alexis, G. Nikolakopoulos, A. Tzes, and L. Dritsas. *Coordination of Helicopter UAVs for Aerial Forest-Fire Surveillance*, pages 169–193. Springer Netherlands, Dordrecht, 2009.

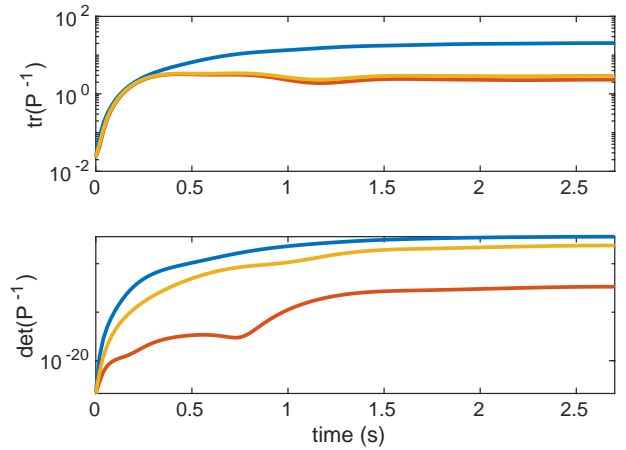


Fig. 2: The traces (top) and determinants (down) of the inverse matrices for the ellipsoidal approximation of FRSs (blue lines). The baseline [18] (brown lines). Proposed method neglecting linearization errors (brown lines). Proposed method considering linearization errors (yellow lines).

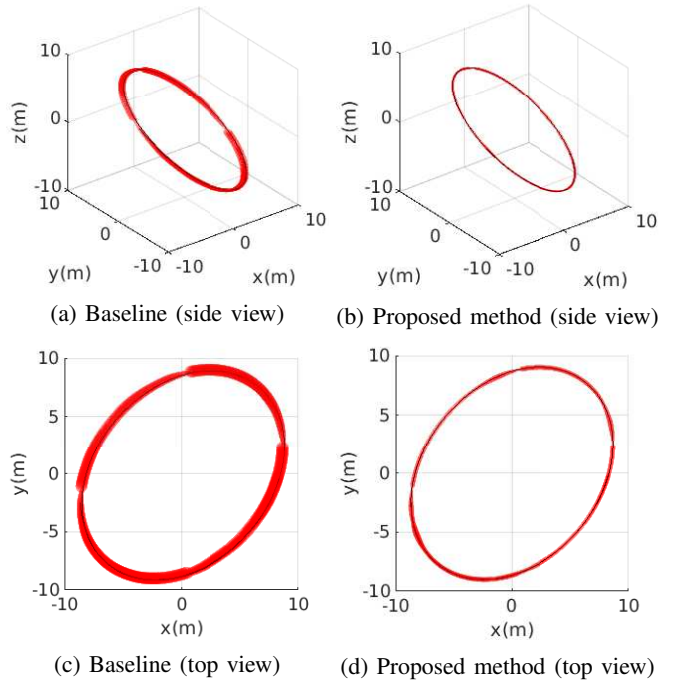


Fig. 3: The side views and top views of FRSs in the position space (red shaded areas) and the trajectory following the circular reference trajectory (black lines) for the baseline [18] and proposed method.

[2] Suseong Kim, Seungwon Choi, and H. Jin Kim. Aerial manipulation using a quadrotor with a two dof robotic arm. In *2013 IEEE/RSJ International Conference on Intelligent Robots and Systems*, pages 4990–4995, 2013.
[3] Steven M. LaValle. *Planning Algorithms*. Cambridge University Press, 2006.
[4] Daniel Mellinger and Vijay Kumar. Minimum snap trajectory generation and control for quadrotors. In *2011 IEEE International Conference on Robotics and Automation*, pages 2520–2525, 2011.

[5] Mark W. Mueller, Markus Hehn, and Raffaello D’Andrea. A computationally efficient motion primitive for quadrocopter trajectory generation. *IEEE Transactions on Robotics*, 31(6):1294–1310, 2015.

[6] I.M. Mitchell, A.M. Bayen, and C.J. Tomlin. A time-dependent hamilton-jacobi formulation of reachable sets for continuous dynamic games. *IEEE Transactions on Automatic Control*, 50(7):947–957, 2005.

[7] Somil Bansal, Mo Chen, Sylvia Herbert, and Claire J. Tomlin. Hamilton-jacobi reachability: A brief overview and recent advances. In *2017 IEEE 56th Annual Conference on Decision and Control (CDC)*, pages 2242–2253, 2017.

[8] Mo Chen, Sylvia L. Herbert, Mahesh S. Vashishtha, Somil Bansal, and Claire J. Tomlin. Decomposition of reachable sets and tubes for a class of nonlinear systems. *IEEE Transactions on Automatic Control*, 63(11):3675–3688, 2018.

[9] Somil Bansal and Claire J. Tomlin. Deepreach: A deep learning approach to high-dimensional reachability. In *2021 IEEE International Conference on Robotics and Automation (ICRA)*, pages 1817–1824, 2021.

[10] Antoine Girard. Reachability of uncertain linear systems using zonotopes. In Manfred Morari and Lothar Thiele, editors, *Hybrid Systems: Computation and Control*, pages 291–305, Berlin, Heidelberg, 2005. Springer Berlin Heidelberg.

[11] Alexander B. Kurzhanski and Pravin Varaiya. Ellipsoidal techniques for reachability analysis. In Nancy Lynch and Bruce H. Krogh, editors, *Hybrid Systems: Computation and Control*, pages 202–214, Berlin, Heidelberg, 2000. Springer Berlin Heidelberg.

[12] Felix Chernousko and Alexander Ovseevich. Properties of the optimal ellipsoids approximating the reachable sets of uncertain systems. *Journal of Optimization Theory and Applications*, 120, 02 2004.

[13] Anirudha Majumdar and Russ Tedrake. Funnel libraries for real-time robust feedback motion planning. *The International Journal of Robotics Research*, 36(8):947–982, 2017.

[14] Suseong Kim, Davide Falanga, and Davide Scaramuzza. Computing the forward reachable set for a multirotor under first-order aerodynamic effects. *IEEE Robotics and Automation Letters*, 3(4):2934–2941, 2018.

[15] Sylvia L. Herbert, Mo Chen, SooJean Han, Somil Bansal, Jaime F. Fisac, and Claire J. Tomlin. Fastrack: A modular framework for fast and guaranteed safe motion planning. In *2017 IEEE 56th Annual Conference on Decision and Control (CDC)*, pages 1517–1522, 2017.

[16] David Fridovich-Keil, Sylvia L. Herbert, Jaime F. Fisac, Sampada Deglurkar, and Claire J. Tomlin. Planning, fast and slow: A framework for adaptive real-time safe trajectory planning. In *2018 IEEE International Conference on Robotics and Automation (ICRA)*, pages 387–394, 2018.

[17] Hoseong Seo, Donggun Lee, Clark Youngdong Son, Claire J. Tomlin, and H. Jin Kim. Robust trajectory planning for a multirotor against disturbance based on Hamilton-Jacobi reachability analysis. In *2019 IEEE/RSJ International Conference on Intelligent Robots and Systems (IROS)*, pages 3150–3157, 2019.

[18] Hoseong Seo, Clark Youngdong Son, Dongjae Lee, and H. Jin Kim. Trajectory planning with safety guaranty for a multirotor based on the forward and backward reachability analysis. In *2020 IEEE International Conference on Robotics and Automation (ICRA)*, pages 7142–7148, 2020.

[19] P. L. Lions and J-C. Rochet. Hopf formula and multitime hamilton-jacobi equations. *Proceedings of the American Mathematical Society*, 96(1):79–84, 1986.

[20] Alireza Mohammadi, Horacio J. Marquez, and Mahdi Tavakoli. Non-linear disturbance observers: Design and applications to euler?lagrange systems. *IEEE Control Systems Magazine*, 37(4):50–72, 2017.

[21] Taeyoung Lee, Melvin Leok, and N. Harris McClamroch. Geometric tracking control of a quadrotor uav on $se(3)$. In *49th IEEE Conference on Decision and Control (CDC)*, pages 5420–5425, 2010.

[22] Taeyoung Lee, Melvin Leok, and N. Harris McClamroch. Control of complex maneuvers for a quadrotor uav using geometric methods on $se(3)$, 2010.

[23] Cécile Durieu, Boris T. Polyak, and Eric Walter. Trace versus determinant in ellipsoidal outer-bounding, with application to state estimation. *IFAC Proceedings Volumes*, 29(1):3975–3980, 1996. 13th World Congress of IFAC, 1996, San Francisco USA, 30 June - 5 July.

[24] Stephen Boyd and Lieven Vandenberghe. *Convex optimization*. Cambridge university press, 2004.

[25] L. Ros, A. Sabater, and F. Thomas. An ellipsoidal calculus based on propagation and fusion. *IEEE Transactions on Systems, Man, and Cybernetics, Part B (Cybernetics)*, 32(4):430–442, 2002.

[26] Hassan K Khalil. *Nonlinear systems*; 3rd ed. Prentice-Hall, Upper Saddle River, NJ, 2002. The book can be consulted by contacting: PH-AID: Wallet, Lionel.

APPENDIX

A. Proof of Lemma 1

Suppose that the function $V_1 = \frac{1}{2}e_d^T e_d$. The time derivative of V_1 derived by (8) is $\dot{V}_1 = -\alpha_d e_d^T e_d + w^T e_d$. The inequality, $\|w\| \leq \|\beta\|$, is satisfied by the *Assumption 1* so that V_1 is developed as

$$\begin{aligned} \dot{V}_1 &\leq -\alpha_d(1 - \theta_1)\|e_d\|^2 - \alpha_d\theta_1\|e_d\|^2 + \|\beta\|\|e_d\| \\ &\leq -2\alpha_d(1 - \theta_1)V_1, \quad \forall\|e_d\| \geq \frac{\|\beta\|}{\alpha_d\theta_1}. \end{aligned} \quad (25)$$

where $0 < \theta_1 < 1$.

The disturbance error e_d converges to a sphere centered to the origin with a radius of $\|\beta\|/\alpha_d\theta_1$ with exponential rate $\alpha_d(1 - \theta_1)$ [26].

B. Proof of Proposition 1

The proof is similar to the proof for the UUB of the controller presented in [14]. Suppose the sum of the functions $V = V_1 + V_2$ such that V_1 is the function in the *Lemma 1* and $V_2 = \frac{1}{2}e_t^T P e_t$ with $e_t = [e_p^T \ e_v^T]^T \in \mathbb{R}^6$ and

$$P = \begin{bmatrix} (k_p + k_v)I_3 & I_3 \\ I_3 & I_3 \end{bmatrix}.$$

From the desired thrust (7) and bounded angle ϕ_b , we derive

$$\|f_d\| \|\sin \phi_b \mathbf{w}\| \leq s_m(k_p\|e_p\| + k_v\|e_v\| + M + \|e_d\|) \quad (26)$$

with $M \in \mathbb{R}^+$ such that $\|ge_3 + \ddot{p}_r + d\| \leq M$ when \ddot{p}_r does not diverge to infinity.

The following inequality related to the time derivative of V is developed by considering (8) and (26):

$$\begin{aligned} \dot{V} &\leq -\mathbf{e}^T Q_1 \mathbf{e} \\ &\quad + \|f_d\| \|\sin \phi_b \mathbf{w}\| (\|e_p\| + \|e_v\|) + \|\beta\|\|e_d\| \\ &\leq -\mathbf{e}^T Q \mathbf{e} + N\|\mathbf{e}\| \end{aligned} \quad (27)$$

with $\mathbf{e} = [\|e_p\| \ \|e_v\| \ \|e_d\|]^T \in \mathbb{R}^3$, $N = \sqrt{2s_m^2M^2 + \|\beta\|^2}$ and $Q = Q_1 + s_m Q_2$. The first and second conditions of the *Proposition 1*, $k_v > 1$ and $\alpha_d > \frac{1}{4}(\frac{1}{k_p} + \frac{1}{k_v-1})$, ensure that Q_1 is positive definite. The last condition, $s_m < -\lambda_{\min}(Q_1)/\lambda_{\min}(Q_2)$, ensures that Q is positive definite despite the fact that Q_2 is not positive definite.

Via a method similar to (25), the inequality (27) becomes

$$\begin{aligned} \dot{V} &\leq -\lambda_{\min}(Q)\|\mathbf{e}\|^2 + N\|\mathbf{e}\| \\ &\leq -\lambda_{\min}(Q)(1 - \theta_2)\|\mathbf{e}\|^2, \quad \forall\|\mathbf{e}\| \geq \frac{N}{\lambda_{\min}(Q)\theta_2} \end{aligned} \quad (28)$$

with $0 < \theta_2 < 1$.

The error dynamics (8) are UUB.